Three-Dimensional Finite Element Analysis of Elastic-Plastic Layered Media Under Thermomechanical Surface Traction

N. Ye, Graduate Student

K. Komvopoulos, Professor, Fellow ASME

Department of Mechanical Engineering
University of California
Berkeley, CA 94720

Abstract

The coupled effects of mechanical and thermal surface traction on the deformation of layered media were analyzed with the finite element method. A three-dimensional model of an elastic spherical asperity sliding over an elastic-plastic layered medium was developed and validated by comparisons of finite element results with analytical and numerical solutions for the surface stresses and temperature distribution on an elastic homogeneous half-space. The evolution of deformation in the layered medium due to thermomechanical surface traction is interpreted in light of the dependence of temperature, von Mises equivalent stress, first principal stress, and equivalent plastic strain on the layer thickness, Peclet number, and sliding distance. The propensity for plastic flow and microcracking in the layered medium is discussed in terms of the layer thickness and thermal properties, sliding speed, medium compliance, and normal load. It is shown that friction and thermal traction promote stress intensification and plasticity, especially in the case of relatively thin layers of low thermal conductivity.

Submitted to the ASME *Journal of Tribology* on January 24, 2002.

1. Introduction

The occurrence of thermal and mechanical traction at sliding interfaces of components is of great importance in a wide range of engineering applications, such as face seals, bearings, automotive brake systems, electric motor brushes, computer head-disk interface, and electrical switches. Catastrophic failure in electromechanical devices is inevitable without fundamental knowledge of the thermomechanical behavior of contacting surfaces. In view of the dependence of the reliability and endurance of various mechanical systems on the response of sliding components to thermomechanical traction, numerous analytical and numerical studies of the temperature rise at sliding interfaces have been conducted, with reference to the pioneering works of Blok (1937) and Jaeger (1942).

Significant advances in analytical and numerical techniques for analyzing material response due to thermomechanical surface traction were encountered in past years. The focus in early studies was the thermal response under constant heat flux and different sliding contact conditions. Kennedy (1981) developed a finite element model to predict the surface temperature in a layered sliding system due to frictional heating and reported a strong effect of the sliding speed on the temperature rise. Tian and Kennedy (1993) determined the temperature rise at sliding contacts for a range of Peclet number using a pseudo three-dimensional model of a coated semi-infinite body and an integral transform method. Vick et al. (1994) adopted a variation of the boundary element method to examine the influence of surface coatings on the temperature due to frictional heating at the sliding contact interface of a layered medium. Tian and Kennedy (1994) used a Green's function method to analyze the temperature rise at the surface of a semi-infinite body due to different moving heat sources.

Thermal and mechanical responses of solids subjected only to thermal loading has been

the objective of several studies. Leroy et al. (1989, 1990) used a fast Fourier algorithm and a two-dimensional finite element model to study the effects of the layer (overcoat) thickness and properties on the temperature and stresses in a layered medium due to a moving heat source. Significantly higher coating stresses were obtained for elastic modulus and thermal expansion coefficient of coating material higher than those of the substrate. Ju and Farris (1997) also used fast Fourier transformation to study the thermal and mechanical response of an elastic half-space due to a moving heat source. However, although in several analyses the mechanical response was determined from the applied thermal load, the distribution area of the heat flux was assumed to be unaffected by the mechanical response.

Most studies dealing with both thermal and mechanical behavior of solids under thermomechanical loading have been based on the finite element technique, evidently due to the complex analytical relations of fully coupled thermomechanical contact problems. Kennedy and Ling (1974) developed a finite element model to study thermal instabilities in disk brakes. Day and Newcomb (1984) performed finite element simulations and experiments to examine the thermomechanical behavior of automotive brakes. However, since the contact pressure and interface region were fixed at each time step to determine the frictional heat and the temperature distribution, this study does not provide a fully coupled thermomechanical analysis. Kulkarni et al. (1991) developed a two-dimensional finite element model for a thermomechanical load translating over an elastic-plastic half-space, and reported results for the temperature distribution, stresses, and plastic strains. Although temperature and displacement fields were solved simultaneously, the thermomechanical load was assumed to be constant despite changes in temperature and displacements. Gupta et al. (1993) used the finite element technique to study two-dimensional rolling and sliding over a semi-infinite half-space under the assumption of

invariant contact pressure with changing temperature. Cho and Komvopoulos (1997) conducted a linear elastic fracture mechanics analysis of subsurface cracking in a homogeneous half-space subjected to moving thermomechanical surface traction and reported that the effect of frictional heating on the crack growth behavior becomes more pronounced with increasing contact friction, crack length-to-depth ratio, and Peclet number.

Previous investigations produced invaluable insight into thermomechanical sliding contact. However, most studies were based on simplistic constitutive models (e.g., purely elastic behavior), ignored the interdependence of thermal and mechanical responses, and assumed constant contact pressure distribution. In sliding contact, the generated frictional heat depends on the contact area and contact pressure profile and vice versa. Therefore, to accurately determine the stress field and contact pressure due to thermomechanical surface traction, it is necessary to use more realistic constitutive models (e.g., elastic-plastic material behavior) and to account for the coupling of thermal and mechanical solutions. Consequently, the main objective of this study was to investigate the thermomechanical response of elastic-plastic media (both homogeneous and layered) under sliding contact. To meet this goal, a three-dimensional fully coupled thermomechanical finite element model was developed, and its accuracy was validated by favorable comparisons of simulation results with analytical solutions from previous studies. Finite element results for the temperature, stresses, and plastic strain in an elastic-plastic layered medium under thermomechanical surface traction are presented for different thickness and thermal conductivity of the layer, Peclet number, and distance (time) from the onset of sliding. The significance of thermal and mechanical traction and the propensity of the layered medium to undergo yielding and cracking are interpreted in the context of simulation results.

2. Finite Element Model

A thermomechanical finite element model was developed to simulate sliding of an elastic spherical asperity of radius R on elastic-perfectly plastic homogeneous and layered media modeled by three-dimensional, eight-node, coupled temperature-displacement finite elements. Due to symmetry, only one-half of the sphere and the medium were modeled in order to reduce the computation time. Figure 1 shows a cross section (x =0) of a typical three-dimensional finite element mesh used in this study, consisting of 13563 elements with a total of 19902 nodes. The normalized mesh dimensions are x/R = 1, y/R = 0.976, and z/R = 3, while those of the homogeneous medium are x/R = 1, y/R = 1.4, and z/R = 3. Plane x = 0 is a symmetry plane, and the positive z-direction coincides with the sliding direction. The nodes on planes x/R = 0 and 1 were fixed against displacement in the x-direction, the nodes on plane y/R = -0.976 were fixed against displacement in the y-direction, and the nodes on planes z/R = -1 and -2 were fixed against displacement in the z-direction. The temperature at the nodes of planes z/R = -1 and 2 was set equal to zero. The top boundary of the mesh (y/R = 0) was thermally insulated except the contact area. The layered medium consists of a layer of thickness h/R = 0.02, 0.05, and 0.1 and a substrate of corresponding thickness h/R = 0.956, 1.3, and 1.3 and different material properties. Thickness and physical properties of the layer and substrate materials are given in Table 1. These data are typical of carbon overcoats and magnetic layers used in hard disks. The asperity properties are identical to those of the layer material (conductivity is fixed at 5.2 W/m $\cdot$ K).

In sliding contact, mechanical energy is transformed to heat due to the friction effect. As frictional heat flows into the interacting bodies, the contact area changes due to thermal expansion affecting the contact pressure distribution. Since these changes in the contact conditions affect the heat generation rate and thermal boundary conditions, the mechanical and

thermal analyses are interdependent and the temperature and stress/strain fields must be determined simultaneously rather than sequentially as in most previous studies. In the present study, the temperature was integrated using a backward-difference scheme $T_{i+1} = T_i + \Delta t \dot{T}_{i+1}$, where T is the temperature and subscript i indicates the ith time step, and the coupled system was solved using Newton's method. The adopted technique automatically invokes an asymmetric matrix storage and solution scheme to improve the convergence history because the stiffness matrix is not symmetric due to friction.

Contact between the sliding asperity and the half-space medium was modeled with contact elements. The contact pressure at a point of the interface p is a function of the "overclosure" δ of the surfaces, i.e.,

$$p = 0, \qquad \text{for } \delta < 0, \qquad \text{(no contact)} \tag{1a}$$

$$p = K\,\delta, \qquad \text{for } \delta \geq 0, \qquad \text{(contact)} \tag{1b}$$

where K is the stiffness in stick, determined through an iterative procedure that satisfies equilibrium. Relations given by Eq. (1) indicate that the contact pressure decreases to zero when the two surfaces are separated, and assumes a nonzero value at contact nodal points. The actual contact pressure depends on the material properties and boundary conditions.

A shear stress τ develops between the contacting surfaces with the occurrence of a very small relative tangential displacement (stick). Macroscopic lateral movement (slip) commences when $\tau = \mu\, p$, where μ is the coefficient of friction. Thus, the stick and slip conditions at the contact interface can be expressed as

$$\tau < \mu\, p \qquad \text{(stick)} \tag{2a}$$

$$\tau = \mu\, p \qquad \text{(slip)} \tag{2b}$$

In all simulation cases, the coefficient of friction specified to the contact elements was set equal to 0.5. The contact area depends on the fraction of energy dissipated during frictional slip in the contacting bodies η and the fraction of heat dissipated into each surface f_1 and f_2, respectively. The heat flux density q_g due to frictional heating is given by

$$q_g = \eta \tau \frac{\Delta s}{\Delta t}, \tag{3}$$

where Δs is the incremental slip and Δt is the incremental time. Heat is instantaneously conducted into each body depending on the values of f_1 and f_2. The contact interface is assumed to have no heat capacity but can exchange heat through conduction.

The heat flux density into the asperity and half-space medium q_1 and q_2, respectively, is given by

$$q_1 = -q_k + f_1 q_g, \tag{4a}$$

and

$$q_2 = q_k + f_2 q_g, \tag{4b}$$

where q_k is the heat flux across the contact interface due to conduction. While the heat flux due to radiation could be taken into account, it was neglected in this study since it is normally much smaller than that due to conduction. When both bodies are at the same temperature, the heat flux into each body is equal to $0.5\,q_g$; however, as the asperity becomes hotter due to continuous sliding, heat conduction q_k occurs across the contact interface (Eq. (4)).

Simulations were performed for $f_1 = f_2 = 0.5$ under the assumption that all frictional energy is dissipated as heat ($\eta = 1$), consistent with Kennedy's finding (1984). It should be noted

that the fraction of heat generated in each body differs from the traditional heat partition factor, which is equal to q_1/q_2.

Heat flux due to conduction is assumed to be of the form

$$q_k = k_g(\theta_1 - \theta_2), \tag{5}$$

where θ_1 and θ_2 are temperatures at surface elements of the sphere and half-space, respectively, and the gap conductance k_g is assumed to be equal to $k/(\Delta l/10)$, where k is the thermal conductivity of the layer material and Δl is the size of the smallest element at the mesh surface. The rationale for the selection of these parameters is the continuity of the temperature across the contact interface. In addition, the produced high gap conductance reduces the sensitivity of the results on the generated heat fractions f_1 and f_2.

Both layer and substrate materials are assumed to exhibit elastic-perfectly plastic material behavior, obeying yield condition

$$\sigma_M = \sqrt{\frac{3}{2} S_{ij} S_{ij}} = \sigma_Y \ , \tag{6}$$

where σ_M is the von Mises equivalent stress, S_{ij} is the deviatoric stress tensor ($S_{ij} = \sigma_{ij} - \sigma_{kk}\delta_{ij}/3$, where σ_{ij} is the stress tensor and δ_{ij} is Knonecker's delta function), and σ_Y is the yield strength in uniaxial tension. The material is assumed to behave as linear elastic until the yield condition is reached. Thereafter, the usual flow rule

$$d\varepsilon_{ij}^p = d\lambda \ S_{ij}, \tag{7}$$

is assumed, where $d\varepsilon_{ij}^p$ is the plastic strain increment and $d\lambda$ is a scalar that depends on the plastic strain rate.

Quasi-static sliding contact simulations were performed with the multi-purpose finite element code ABAQUS using six steps, each having 8-23 increments. The simulations comprised indentation of the half-space by the asperity (at $z/R = 0$) to a depth corresponding to a fixed normal load, followed by five incremental displacements $\Delta z/R = 0.05$, 0.15, 0.35, 0.65, and 0.95 of the asperity under the given load in the z direction. The typical computational time on a Pentium III 550 PC was about 55040 CPU seconds.

3. Model Validation

Normal contact simulations with and without frictional heating were performed in order to evaluate the appropriateness of the finite element model. Figure 2 shows a comparison between finite element results and analytical solutions (Huber, 1904) for elastic homogeneous half-space with properties those of the layer material (Table 1) indented by a rigid sphere. The stresses are normalized by the maximum contact pressure p_0 and coordinate z by the contact radius r. The figure shows that the variations of the normal stress components at the surface along the z-direction ($x = y = 0$) predicted by the two methods are in good agreement. Results for the surface temperature distribution obtained from a thermomechanical finite element analysis of an asperity sliding over an elastic homogeneous half-space are shown in Fig. 3 ($\eta = 1$, and $\mu = 0.5$). The figure shows the evolution of the surface temperature T with time for Peclet number $Pe = 30$ ($Pe = vr/\alpha$, where v is the sliding speed and α is the thermal diffusivity). In this figure, as well as in subsequent figures, the temperature is normalized by $2rq_m/k$, where q_m is the average heat flux into the medium and k is the thermal conductivity, and time t is normalized by t_0, which is the time corresponding to a sliding distance equal to the contact radius. The z-coordinate of the asperity center is denoted by z_0. The maximum temperature increases with time and its location

shifts gradually toward the trailing edge of the contact region due to the effect of the moving heat source (asperity). This trend and magnitude of peak temperature (Fig. 3) are in fair agreement with the analysis of Tian and Kennedy (1994). Favorable comparisons of the results shown in Figs. 2 and 3 with those of other studies demonstrate the suitability of the finite element model and the appropriateness of the assumed boundary conditions for thermomechanical sliding contact analysis.

4. Results and Discussions

In this section, finite element solutions for temperature, stress, and strain fields in a layered medium subjected to thermal and mechanical surface traction are interpreted in terms of the thickness and thermal conductivity of the layer, Peclet number, and distance of sliding. All simulation results presented below were obtained for $\eta = 1$ (unless stated otherwise) and $\mu = 0.5$. The significance of frictional heating and tangential (friction) traction on the deformation behavior, in particular the tendency for yielding and cracking in the layered medium, is elucidated in light of stress and strain results.

Figures 4 illustrates the effect of frictional heating on the distribution and maximum value of the von Mises equivalent stress in a homogeneous elastic-plastic half-space with properties those of the layer material (Table 1, k = 0.052 W/m·K) for Pe = 30 and η = 0 and 1. The maximum indentation load and penetration depth during sliding were the same in both thermomechanical (η = 1) and mechanical (η = 0) simulation cases. The maximum von Mises equivalent stress occurred always at the surface. This is consistent with analytical results of Hamilton (1983) and Sackfield and Hills (1983) demonstrating that the maximum von Mises stress is always encountered at the surface when $\mu > 0.3$. However, frictional heating was found

to affect the location of the peak Mises stress at the surface. For $\eta = 0$, the peak Mises stress occurred near the front edge of the contact region (i.e., $z > z_0$, where z_0 is the z coordinate of the asperity center), whereas for $\eta = 1$, it occurred at the center of contact ($z = z_0$). For $\eta = 1$, the temperature at the contact interface rises as the sphere slides over the medium, leading to thermal expansion of both sphere and half-space media. Figure 4(a) shows that growth of the contact region due to thermal expansion affected the steady-state contact stress distribution ($t/t_0 = 6.5$). Moreover, as shown in Fig. 4(b), the effect of frictional heating is negligible during indentation, evidently due to the very small relative slip at the contact interface. Under purely mechanical traction ($\eta = 0$), the maximum Mises stress increases rapidly with the onset of sliding, reaching a peak at sliding distance approximately equal to the contact radius ($t/t_0 = 1$). However, when frictional heating occurs simultaneously with mechanical loading at the contact interface ($\eta = 1$), the maximum Mises stress continues to increase during sliding, thus increasing the probability for yielding at the contact interface. Since the thermal effect on the contact stress field becomes more pronounced with increasing Peclet number, surface plasticity is more likely to occur at interfaces of components involving high sliding speeds, low diffusivity materials, high normal loads, and high-compliance interfaces producing large contact areas.

Temperature results for a layered medium with properties given in Table 1 ($h/R = 1.3$ (substrate); $h/R = 0.1$ and $k = 5.2$ W/m·K (layer)) subjected to both thermal and mechanical traction are shown in Fig. 5 for $Pe_L = 0.29$. The Peclet number is obtained in terms of the thermal diffusivity of the layer $\alpha_L = (k/\rho c)_L$, where ρ and c are the density and heat capacity of the layer material, respectively. The temperature is normalized by the thermal conductivity of the substrate k_s. Figures 5(a) and 5(b) show the temperature evolution at the surface ($y/h = 0$) and interface ($y/h = -1$) of the layered medium, respectively. A steady-state surface temperature profile is obtained

after reaching a sliding distance of about four times the contact radius (i.e., t/t_0 = 4.62), in agreement with the findings of another study (Kennedy, 1981). Figure 5(b) shows that the interface temperature is significantly lower than that at the surface. The main reason is the very low thermal conductivity of the layer (~5.3 percent that of the substrate). This is the case of a thermally conductive substrate coated with an insulating material. Thus, the small fraction of frictional heat reaching the layer interface is effectively conducted into the substrate yielding an interface temperature an order of magnitude less than that at the surface.

Figures 6 and 7 show the effect of layer properties and thickness on the maximum temperature rise at the surface and interface of the elastic-plastic layered medium. Three cases of different layer thermal conductivity (k_L = 0.052, 0.52, and 5.2 W/m·K) and fixed thickness (h/R = 0.02 (layer) and 0.956 (substrate)), and three cases of fixed layer thermal conductivity (k_L = 5.2 W/m·K) and different layer thickness (h/R = 0.02, 0.05, and 0.1, and corresponding substrate thickness h/R = 0.956, 1.3, and 1.3) were simulated for the same normal load and sliding velocity. The maximum surface temperature increases with Peclet number (Fig. 6(a)), thus increasing the probability for thermal cracking at the surface of the layered medium, while the temperature at the interface exhibits an opposite trend (Fig. 6(b)). The increase of Pe_L can be associated with higher sliding speed, larger conduct radius, and lower diffusivity materials. Hence, in the case of a fast moving heat source (asperity microcontact) and/or insulating layer material, heat conduction through the layer is prevented and high temperatures are encountered only at the contact region. A similar trend is observed with increasing layer thickness (Fig. 7). However, considering the change in temperature versus range of Peclet number and layer thickness, it is concluded that the effect of the layer thickness is significantly more pronounced than that of the layer thermal conductivity. Therefore, a thicker and less conductive layer is more

effective in protecting the substrate from thermal softening and phase transformation (annealing), although under certain circumstances this might have an adverse effect on the protective layer.

To examine the effect of the layer thickness and properties on the likelihood of yielding and cracking in the layered medium due to thermomechanical traction ($\eta = 1$), the maximum von Mises equivalent stress $\sigma_M^{\max} / p_0$, maximum first principal stress $\sigma_I^{\max} / p_0$, and maximum equivalent plastic strain $\varepsilon_p^{\max}$ are plotted in Figs. 8 and 9 in terms of sliding time t/t_0 and layer thickness h/R. Stresses are normalized by the peak pressure p_0 corresponding to $h/R = 0.1$ and $t/t_0 = 0$. Open (filled) symbols in Fig. 8 denote the layer surface (interface), while open (filled) symbols in Fig. 9 denote the bulk (interface) of the substrate. The same normal load was used in all simulation cases. Both $\sigma_M^{\max}$ and $\sigma_I^{\max}$ increase rapidly with the onset of sliding in both layer and substrate media, evidently due to the development of shear traction, reaching steady-state values at sliding distances of 2-6 times the contact radius, depending on the layer thickness. The significantly higher maximum von Mises and first principal stresses obtained with relatively thin layers indicate a greater propensity for thin overcoats to undergo plastic deformation and cracking due to thermomechanical surface traction.

The layer thickness plays an important role on the location of $\sigma_M^{\max}$ and $\sigma_I^{\max}$. For relatively thin layers ($h/R = 0.02$), sliding causes $\sigma_M^{\max}$ to shift from the surface to the layer interface (Fig. 8(a)), while $\sigma_I^{\max}$ occurs always at the layer surface (Fig. 8(b)). For layers of intermediate ($h/R = 0.05$) or large ($h/R = 0.1$) thickness, an opposite trend is observed after the onset of sliding ($t/t_0 > 1$), i.e., the location of $\sigma_M^{\max}$ eventually shifts from the interface to the surface of the layer, indicating a significant friction (thermal) effect on the location where plasticity commences first in the layer (Fig. 8(a)). However, the location of $\sigma_I^{\max}$ (interface) for

h/R = 0.02 and 0.05 is not affected by the shear and thermal traction resulting from sliding contact (Fig. 8(b)).

Regarding deformation in the substrate, it was found that plastic deformation during sliding always commenced at the interface (Fig. 9(b)). (For the range of layer thickness, material properties, and normal load analyzed, plasticity was confined in the substrate for all simulation cases.) The magnitude of $\varepsilon_p^{\max}$ increases as the layer thickness decreases, suggesting a greater likelihood for plastic flow in the substrate in the case of thinner overcoats. In addition, the thinner layer produces a higher maximum tensile stress at the layer/substrate interface (Fig. 9(a)). The shift of $\sigma_1^{\max}$ from the bulk of the substrate to the interface illustrates the effect of shear and thermal traction on the location where microcracking is likely to occur in the substrate material. The results shown in Figs. 8 and 9 demonstrate the important role of the layer thickness on the resistance against plastic deformation and cracking of layered media subjected to thermomechanical surface traction.

5. Conclusions

A thermomechanical finite element analysis for sliding contact of layered media was performed in order to elucidate the role of the surface layer (overcoat) material properties and thickness on the evolution of temperature, stress, and strain fields. The finite element model accounts for elastic-plastic deformation and conduction of frictional heat in both contacting solids. Based on the presented results and discussion, the following main conclusions can be drawn.

(1) A three-dimensional model for thermomechanical contact analysis was developed and validated by comparisons of simulation results with solutions from an elastic normal contact

analysis and temperature rise results from a thermomechanical numerical analysis of sliding contact.

(2) A steady-state temperature distribution is reached at the layer surface and layer/substrate interface at sliding distances equal to 4-6 times the contact radius.

(3) The layer thickness exhibits a more pronounced effect on the interface temperature rise, while the influence of the Peclet number (i.e., layer thermal properties, sliding speed, medium compliance, and normal load) is relatively secondary.

(4) Frictional heating coupled with shear surface traction in sliding contact may intensify the stress field in layered media significantly. The likelihood for yielding and cracking increases with decreasing layer thickness. The location of the maximum von Mises equivalent stress, maximum tensile stress, and maximum equivalent plastic strain depends on the layer thickness and the frictional heat conducted through the layer, controlled by the thermal conductivity of the layer material, coefficient of friction, contact interface compliance, and normal load.

Acknowledgments

This research was partially supported by the National Storage Industry Consortium (NSIC), Extremely High Density Recording (EHDR) Program, and the Computer Mechanics Laboratory at the University of California at Berkeley.

References

Blok, H., 1937, "Theoretical Study of Temperature Rise at Surfaces of Actual Contact Under Oiliness Lubricating Conditions," *Proceedings Institute of Mechanical Engineers, General Discussion of Lubrication*, **2** pp. 222-235.

Cho, S.-S., and Komvopoulos, K., 1997, "Thermoelastic Finite Element Analysis of Subsurface Cracking Due to Sliding Surface Traction," ASME *Journal of Engineering Materials and Technology*, **119**, pp. 71-78.

Colin, F., Floquet, A., and Play, D., 1988, "Thermal Contact Simulation in 2-D and 3-D Mechanisms," ASME *Journal of Tribology*, **110**, pp. 247-252.

Day, A. J., and Newcomb, T. P., 1984, "The Dissipation of Frictional Energy from the Interface of an Annular Disc Brake," *Proceedings Institution of Mechanical Engineers*, **198D**, pp. 201-209.

Graebner, J. E., 1994, "Measurements of Specific Heat and Mass Density in CVD Diamond," *Diamond and Related Materials*, **5**, pp. 1366-1370.

Gupta, V., Bastias, P., Hahn, G. T., and Rubin, C. A., 1993, "Elasto-Plastic Finite-Element Analysis of 2-D Rolling-Plus-Sliding Contact with Temperature-Dependent Bearing Steel Material Properties," *Wear*, **169**, pp. 251-256.

Hamilton, G. M., 1983, "Explicit Equations for the Stresses Beneath a Sliding Spherical Contact," *Proceedings of the Institution of Mechanical Engineers Part C – Journal of Mechanical Engineering Science*, **197**, pp. 53-59.

Huang, J. H., and Ju, F. D., 1985, "Thermomechanical Cracking Due to Moving Friction Loads," *Wear*, **102**, pp. 81-104.

Huber, M. T., 1904, "Zur Theorie der Beruhrung Fester elasticher Korper," *Annalen der Physik*, **14**, pp. 153-163.

Jaeger, J. C., 1942, "Moving Sources of Heat and the Temperature at Sliding Contacts," *Proceedings Royal Society of NS Wales*, **76**, pp. 203-224.

Ju, Y., and Farris, T. N., 1997, "FFT Thermoelastic Solutions for Moving Heat Sources," ASME *Journal of Tribology*, **119**, pp. 156-162.

Ju, F. D., and Liu, J. C., 1988, "Effect of Peclet Number in Thermo-Mechanical Cracking Due to High-Speed Friction Load," ASME *Journal of Tribology*, **110**, pp. 217-221.

Kennedy, F. E., and Ling, F. F., 1974, "A Thermal, Thermoelastic, and Wear Simulation of a

High Energy Sliding Contact Problem," ASME *Journal of Lubrication Technology*, **97**, pp. 497-507.

Kennedy, F. E., 1981, "Surface Temperatures in Sliding Systems – A Finite Element Analysis," *ASME Journal of Lubrication Technology*, **103**, pp. 90-96.

Kennedy, F. E., 1984, "Thermal and Thermomechanical Effects in Dry Sliding," *Wear*, **100**, pp. 453-476.

Kulkarni, S. M., Rubin, C. A., and Hahn, G. T., 1991, "Elasto-Plastic Coupled Temperature-Displacement Finite Element Analysis of Two-Dimensional Rolling-Sliding Contact With a Translating Heat Source," ASME *Journal of Tribology*, **113**, pp. 93-101.

Leroy, J. M., Floquet, A., and Villechaise, B., 1989, "Thermomechanical Behavior of Multilayered Media: Theory," ASME *Journal of Tribology*, **111**, pp. 538-544.

Leroy, J. M., Floquet, A., and Villechaise, B., 1990, "Thermomechanical Behavior of Multilayered Media: Results," ASME *Journal of Tribology*, **112**, pp. 317-323.

Morath, C. J., and Maris, H. J., 1994, "Picosecond Optical Studies of Amorphous Diamond and Diamondlike Carbon: Thermal Conductivity and Longitudinal Sound Velocity," *Journal of Applied Physics*, **76**, pp. 2636-2640.

Sackfield, A. and Hills, D. A., 1983, "A Note on the Hertz Contact Problem: A Correlation of Standard Formulas," *Journal of Strain Analysis for Engineering Design*, **18**, pp. 195-197.

Tian, X., and Kennedy, F. E., 1993, "Temperature Rise at the sliding Contact Interface for a Coated Semi-Infinite Body," ASME *Journal of Tribology*, **115**, pp. 1-9.

Tian, X., and Kennedy, F. E., 1994, "Maximum and Average Flash Temperature in Sliding Contacts," ASME *Journal of Tribology*, **116**, pp. 167-174.

Vick, B., Golan, L. P., and Furey, M. J., 1994, "Thermal Effects Due to Surface Films in Sliding Contact," ASME *Journal of Tribology*, **116**, pp. 238-246.

Table 1. Thickness and properties of layer and substrate media of the finite element model[a]

Medium	Layer	Substrate
Thickness, h/R	0.02, 0.05, 0.1	0.956, 1.3, 1.3
Elastic modulus, E (GPa)	168	130
Poisson ratio, □	0.3	0.3
Yield strength, $\square_Y$ (GPa)	13	2.67
Conductivity, k (W/m · K)	0.052, 0.52, 5.2	98
Specific heat, c (J/g · K)	0.5	0.42
Density, □ (kg/m^3)	2150	8800
Thermal expansion, a (K^{-1}	2 x 10^{-6}	13 x 10^{-6}
Thermal diffusivity, □ (m	4.837 x 10^{-6}	26.52 x 10^{-6}

[a]The elastic modulus and thermal modulus of the asperity are identical to those of the layer material.

List of Figures

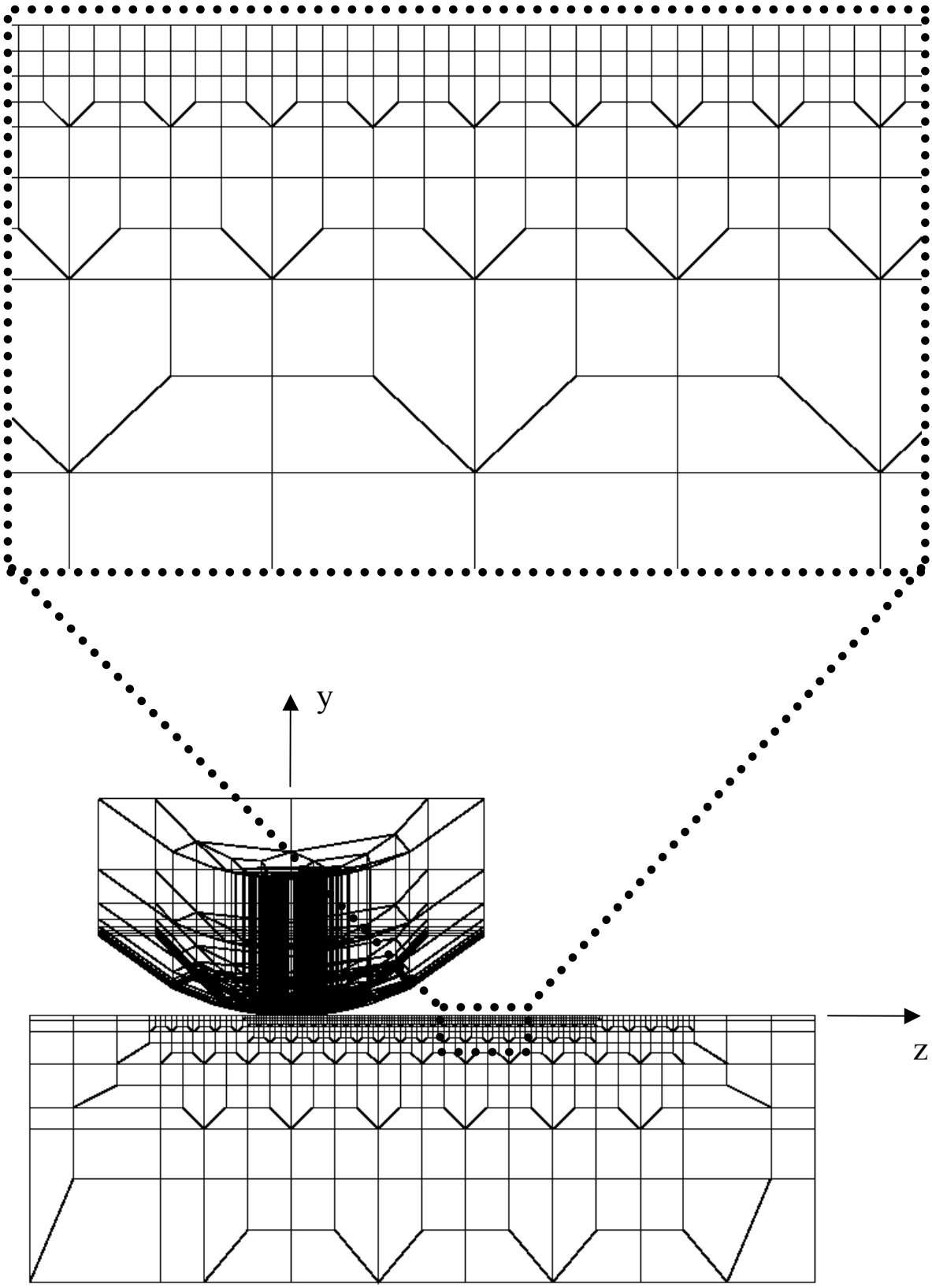

Figure 1

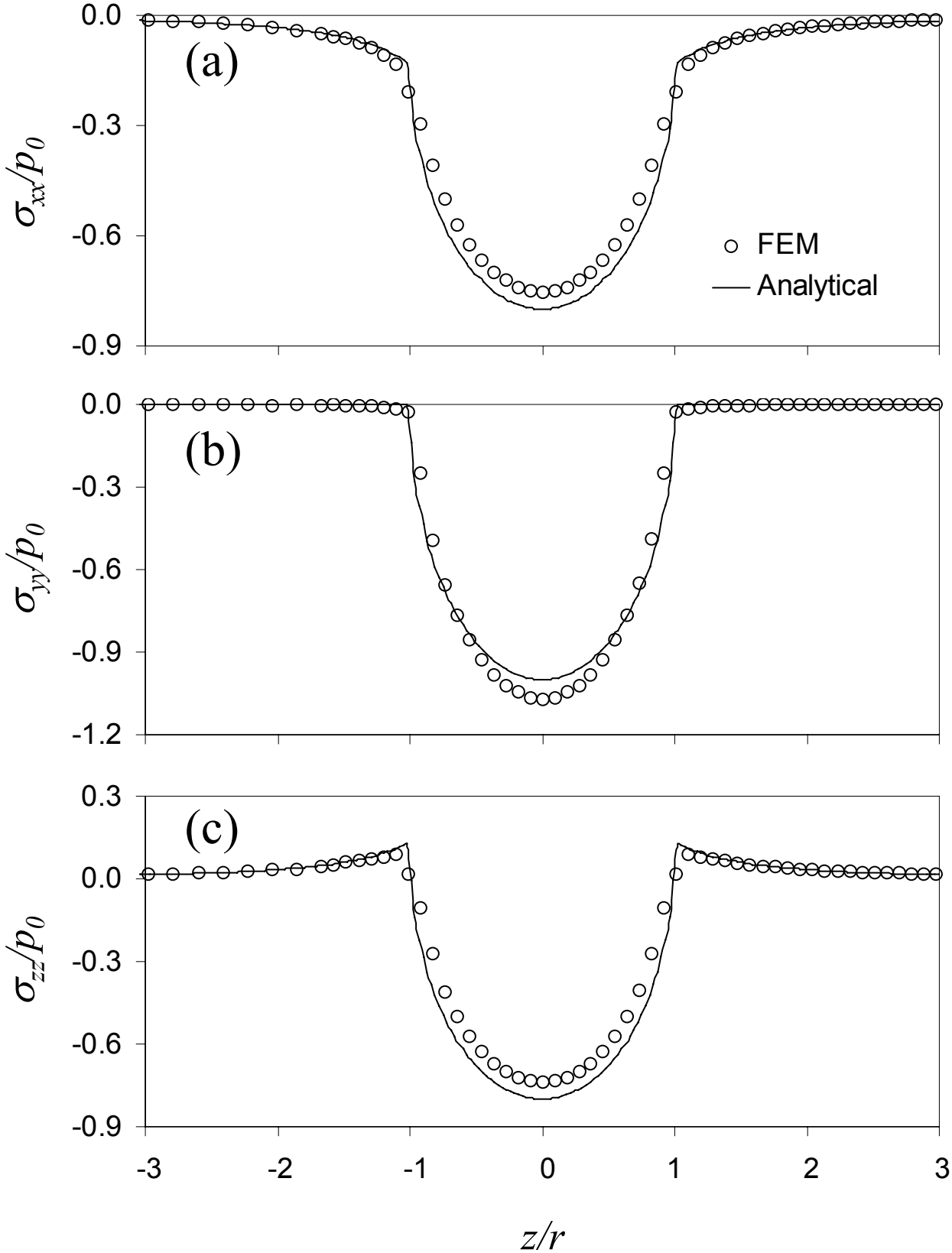
(a)
(b)
(c)
FEM
Analytical
σ_{xx}/p_0
σ_{yy}/p_0
σ_{zz}/p_0
0.0
-0.3
-0.6
-0.9
-1.2
0.3
-3
-2
-1
0
1
2
3
z/r

Figure 2

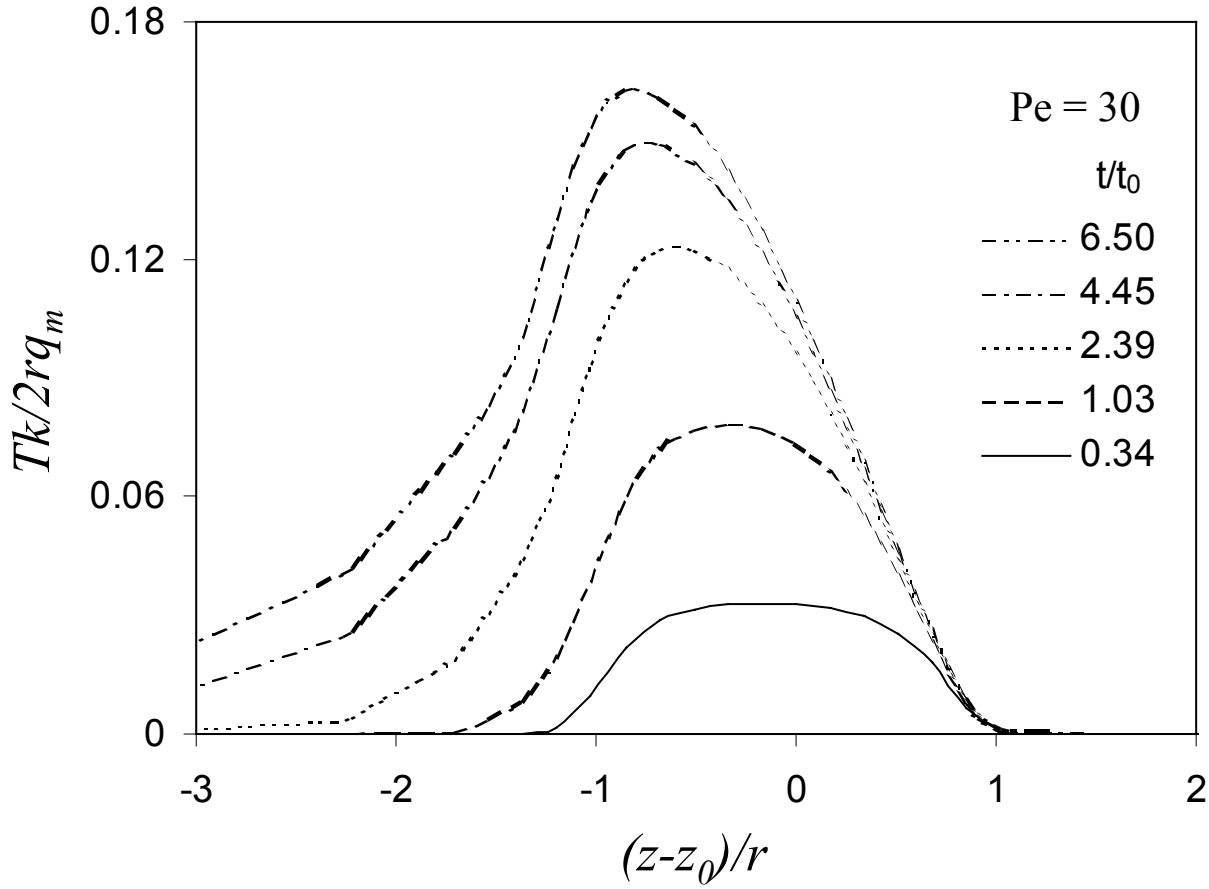

Figure 3

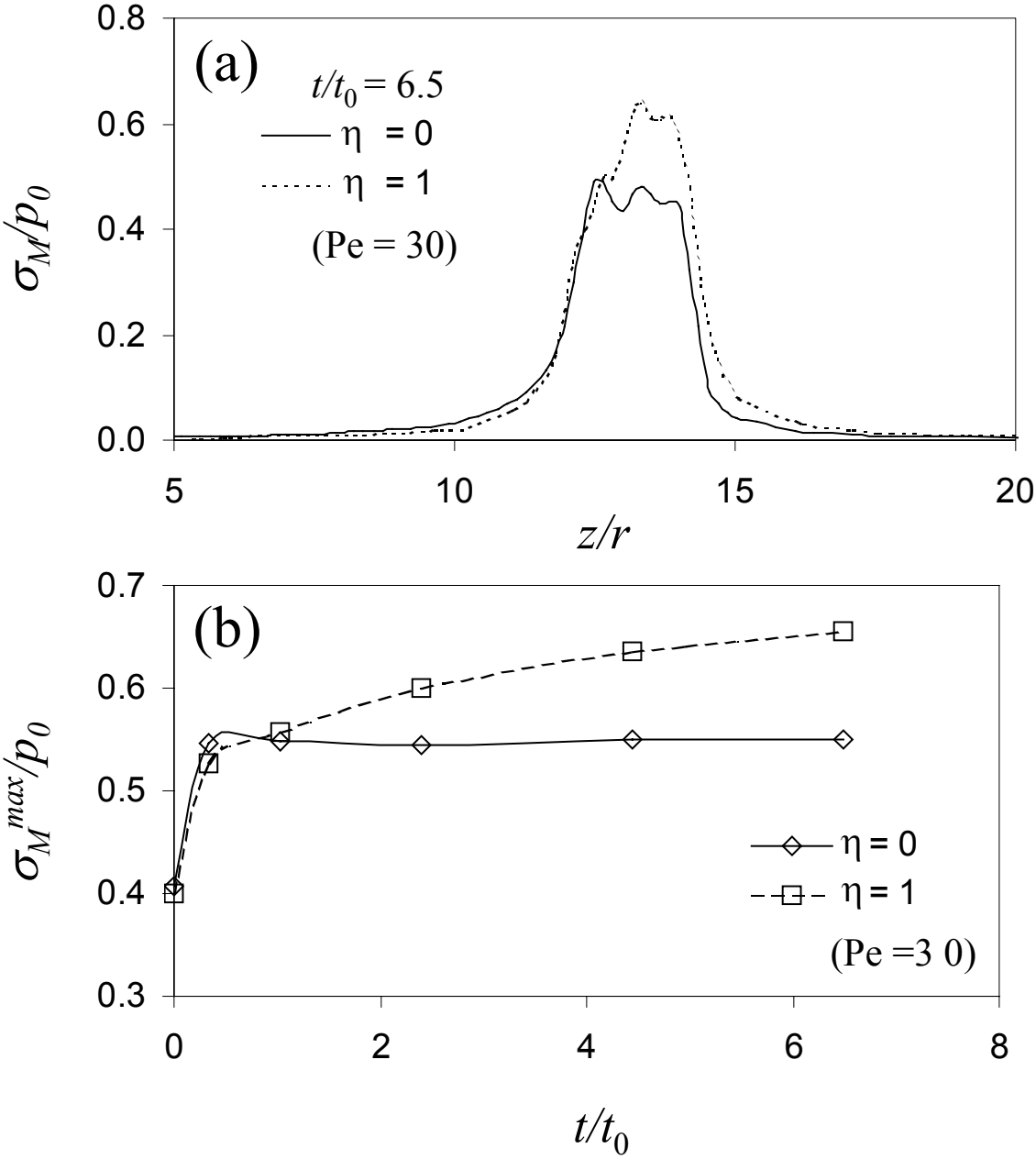
(a)
$t/t_0 = 6.5$
η = 0
η = 1
(Pe = 30)
σ_M/p_0
z/r
0.0
0.2
0.4
0.6
0.8
5
10
15
20
(b)
σ_M^{max}/p_0
t/t_0
η = 0
η = 1
(Pe =3 0)
0.3
0.4
0.5
0.6
0.7
0
2
4
6
8

Figure 4

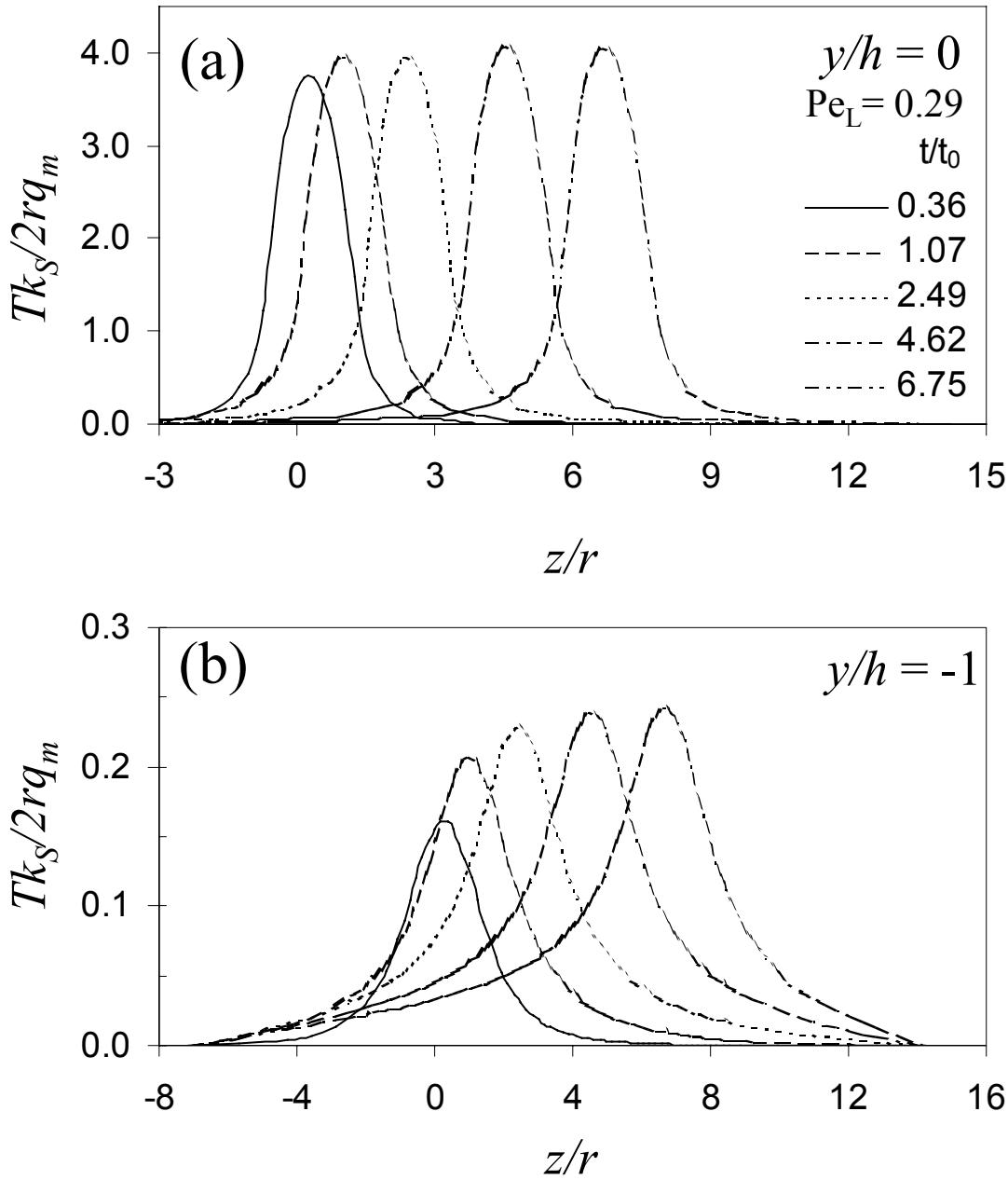
(a)
y/h = 0
Pe_L = 0.29
t/t0
0.36
1.07
2.49
4.62
6.75
Tk_S/2rq_m
z/r
(b)
y/h = -1
Tk_S/2rq_m
z/r

Figure 5

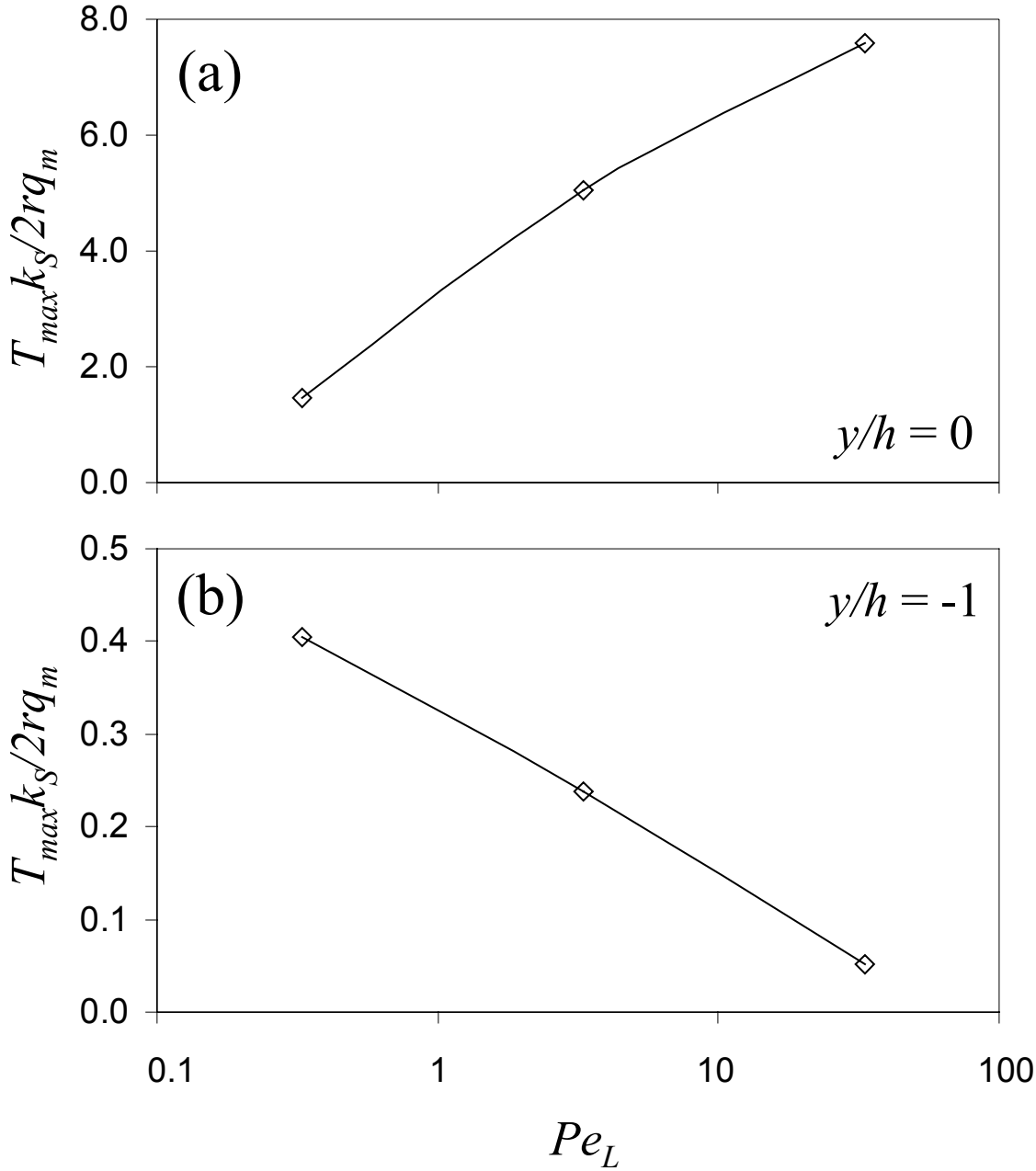
(a)
8.0
6.0
4.0
2.0
0.0
$T_{max}k_S/2rq_m$
$y/h = 0$
(b)
0.5
0.4
0.3
0.2
0.1
0.0
$T_{max}k_S/2rq_m$
$y/h = -1$
0.1
1
10
100
Pe_L

Figure 6

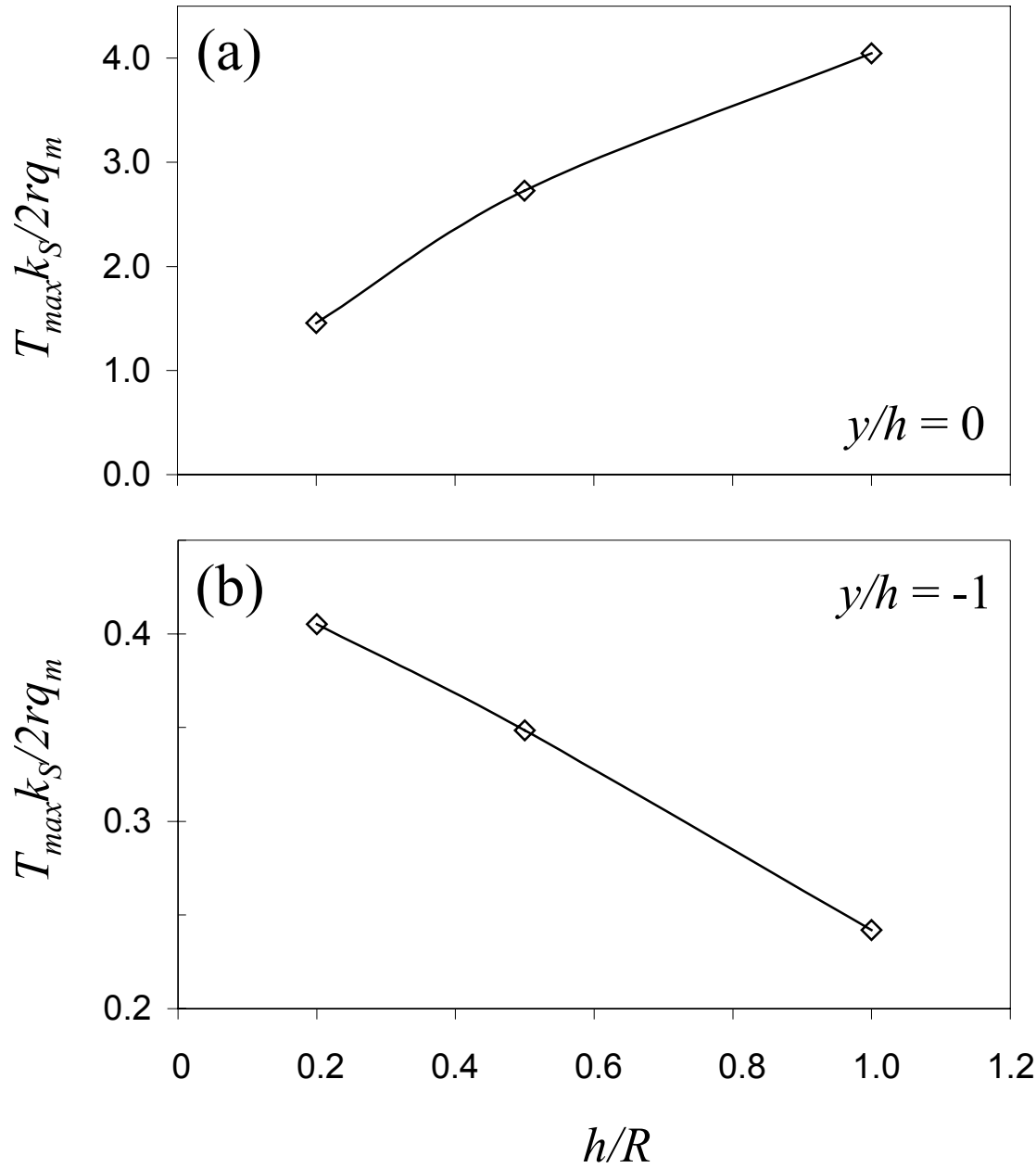
(a)
4.0
3.0
2.0
1.0
0.0
$T_{max}k_S/2rq_m$
$y/h = 0$
(b)
$y/h = -1$
0.4
0.3
0.2
$T_{max}k_S/2rq_m$
0
0.2
0.4
0.6
0.8
1.0
1.2
h/R

Figure 7

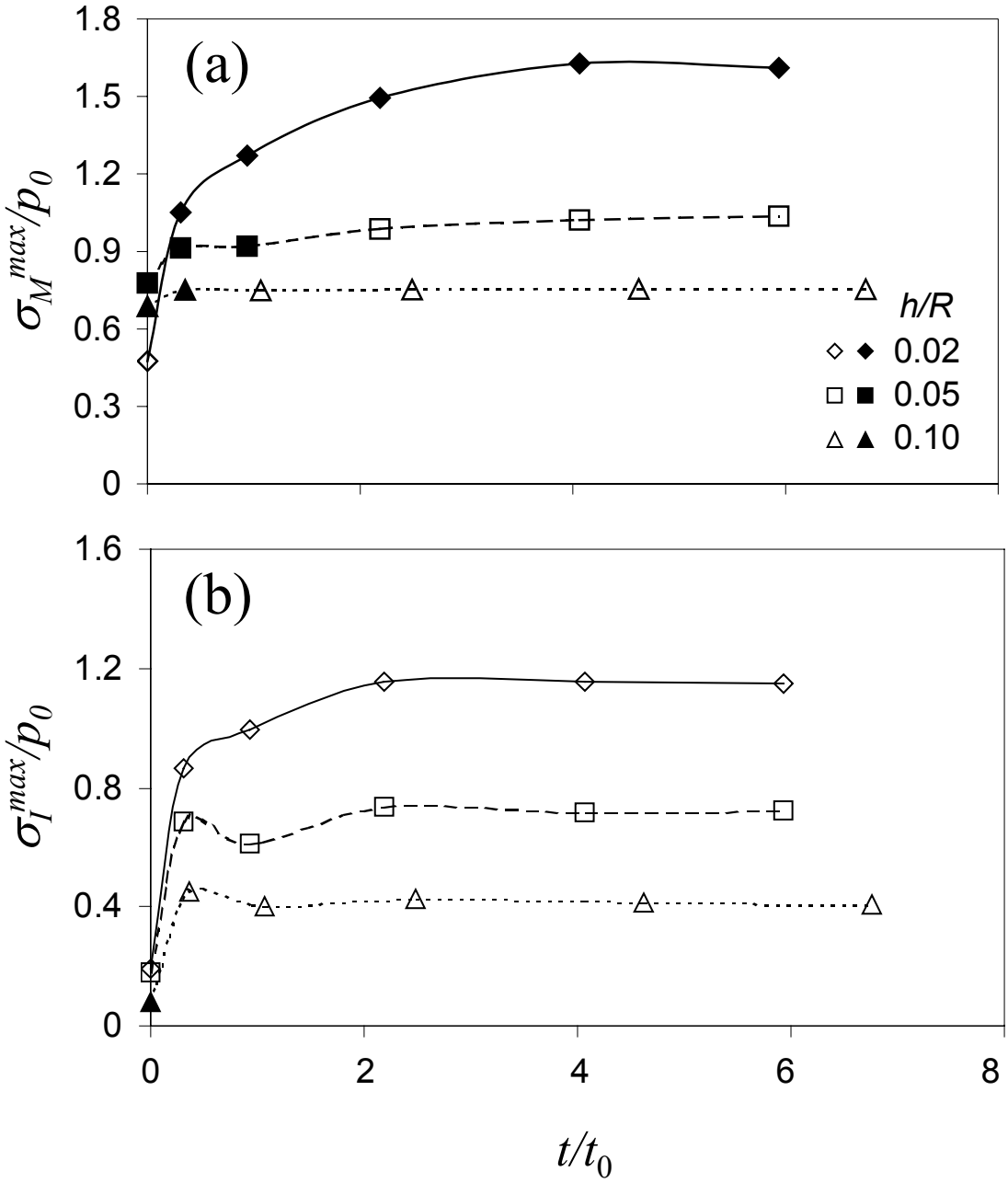
(a)
(b)
σ_M^{max}/p_0
σ_I^{max}/p_0
t/t_0
h/R
0.02
0.05
0.10
1.8
1.5
1.2
0.9
0.6
0.3
0
1.6
1.2
0.8
0.4
0
2
4
6
8

Figure 8

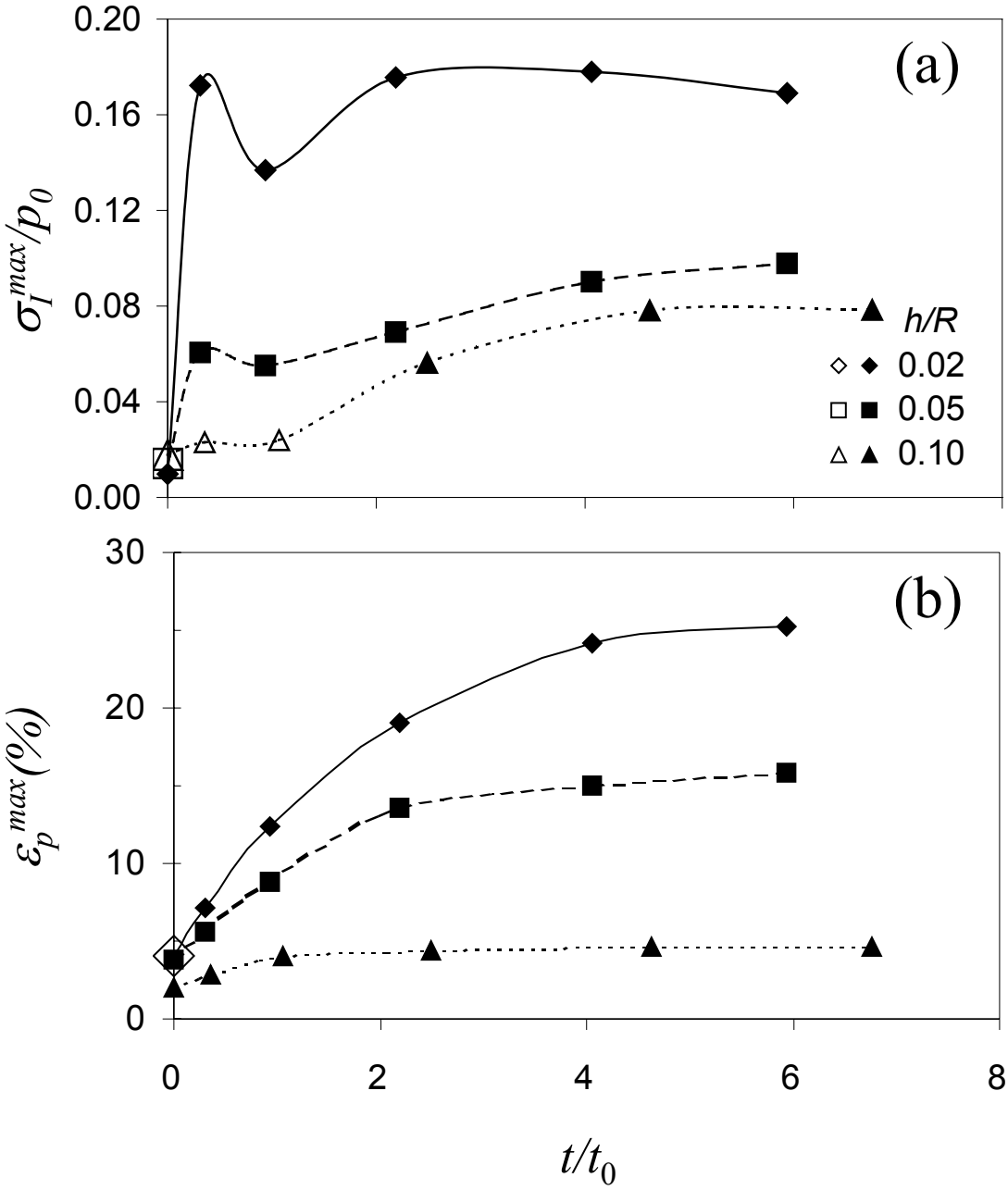
(a)
(b)
σ_I^{max}/p_0
$\varepsilon_p^{max}(\%)$
t/t_0
h/R
0.02
0.05
0.10
0.00
0.04
0.08
0.12
0.16
0.20
0
10
20
30
0
2
4
6
8

Figure 9